Prediction of Dry-Season Precipitation in Tropical West Africa and its Relation to Forcing from the Extratropics

Peter Knippertz
Institute for Atmospheric Physics, Johannes Gutenberg University Mainz, Mainz, Germany

Andreas H. Fink
Institute of Geophysics and Meteorology, University of Cologne, Cologne, Germany

NOTE: This is the Accepted Version from January 26, 2009

Revised version for

Weather and Forecasting

January 2009

Corresponding author address: Peter Knippertz, Institut für Physik der Atmosphäre, Johannes Gutenberg-Universität Mainz, 55099 Mainz, Germany.
E-mail: knippertz@uni-mainz.de

ABSTRACT

Precipitation during the boreal winter dry season in tropical West Africa is rare but occasionally connected to high-impacts for the local population. The dynamics and predictability of this phenomenon have been studied very little. Here a statistical evaluation of the climatology, dynamics, and predictions of dry-season wet events is presented for the region 7.5–15°N, 10°W–10°E. The analysis is based upon GPCP merged satellite-gauge pentad rainfall estimates and five-day ERA-40 precipitation forecast, and covers the 23 dry seasons (November–February) 1979/80–2001/02. Wet events are defined as pentads with an area-averaged precipitation anomaly of more than +200% with respect to the mean seasonal cycle. Composites of the 43 identified events indicate an association with a trough over northwestern Africa, a tropical plume on its eastern side, unusual precipitation at the northern and western fringes of the Sahara, and reduced surface pressure over the Sahara, which allows an inflow of moist southerlies from the Gulf of Guinea to feed the unusual dry-season rainfalls. The results give evidence for a pre-conditioning by another disturbance about one week prior to the precipitation event. The ERA-40 forecasts show a high temporal correlation with observations, a general wet bias, but a somewhat too low number of wet events. With 53% of all identified events correctly forecasted and only 32% of forecasted events not verified the model shows a moderate skill in contrast to the prediction of many other tropical precipitation systems. A separate consideration of hits, misses, and false alarms corroborates the previously proposed hypothesis that a strong extratropical influence enhances the quality of predictions in this region. The results should encourage weather services in West Africa to take advantage of available dry-season precipitation forecasts in terms of the dissemination of early warnings.

1. Introduction

During boreal winter tropical West Africa is under the influence of dry and often dusty northeasterly Harmattan winds from the Sahara. Regular rainfalls are absent, except for the coastal strip between the Grain Coast and the Niger Delta (e.g., Buckle 1996). Occasional dry-season precipitation events in the Soudano-Sahelian zone of West Africa have been termed Mango or Heug rains in the western part and are often related to upper-level disturbances intruding from the extratropical North Atlantic into the Tropics (Seck 1962; Griffiths 1972; Borgne 1979; Gaye et al. 1994; Issar 1995; Buckle 1996; Leroux 2001). Recently Knippertz and Fink 2008a (KF08 hereafter) documented a case of an unusual northward penetration of the rain zone into the countries of Ghana, Togo, Benin, and Nigeria in January 2004. Despite their rare occurrence, dry-season wet events can have substantial impacts on the local hydrology and human activities reaching from greening pastures to flooding and rotting harvests (Knippertz and Martin 2005; Fall et al. 2007; KF08). KF08 proposed a close link of the unusual tropical rainfalls to the synoptic evolution in the extratropics. They show that extratropical disturbances penetrating into low latitudes support a diabatic pressure fall over West Africa through the anomalous radiative warming under a diagonal cloud band on the eastern flank of a first trough, often referred to as a tropical plume (TP; see Knippertz 2005), and a dynamical pressure fall through subsidence and warm advection associated with a subsequent second upper-level trough. As a consequence of the reduced surface pressure, moist monsoon air from the Gulf of Guinea penetrates inland and allows the formation of deep moist convection and heavy precipitation. In the case discussed by KF08, extreme precipitation also occurred in subtropical Northwest Africa to the east of the second trough.

Based on this case study KF08 hypothesized that the strong extratropical influences may imply a comparably good predictability of such events that would allow a timely warning of the population and therefore a mitigation of detrimental impacts as well as an exploitation of beneficial effects. To test this hypothesis, the present study gives a statistical evaluation of boreal winter precipitation forecasts made by the European Centre for Medium-Range Weather Forecasts (ECMWF) as part of the ERA-40 project (Uppala et al. 2005). Only the geostationary satellite period from 1979–2002, usually regarded as the more reliable part of the dataset for climatological analyses (Kållberg et al. 2005), will be considered. The objectives of this study are (A) to identify episodes of a temporary northward extension of the ITCZ rainfall belt onto the West African continent during the dry season (November–February), (B) to understand the dynamics of the rainfall generation including the role of the extratropics, (C) to evaluate the ability of a state-of-the-art numerical weather prediction (NWP) model to forecast such events, and (D) to investigate in what way the degree of extratropical influence is related to forecast skill. The remainder of the paper is structured as follows. Section 2 provides information on the employed observational and forecast data. Section 3 contains an exemplary case study. Section 4 describes the identification of dry-season wet events and their climatology, while section 5 evaluates ERA-40 forecasts of these events. Section 6 contains a detailed analysis of the dynamics including a differentiation between successful and unsuccessful forecasts. The most important results are summarized and discussed in section 7 together with a compilation of open research issues.

2. Data

a. Precipitation observations

The main observational dataset used in this study is a merged satellite-gauge product provided by the Global Precipitation Climatology Project (GPCP). This dataset includes microwave precipitation estimates based on Special Sensor Microwave/Imager (SSM/I) data from the polar-orbiting Defense Meteorological Satellite Program (DMSP) satellites and infrared (IR) precipitation estimates from geostationary and polar-orbiting satellites. Additional low-Earth orbit estimates include the Atmospheric Infrared Sounder (AIRS) data from the NASA Aqua, and Television Infrared Observation Satellite Program (TIROS) Operational Vertical Sounder (TOVS) and Outgoing Longwave Radiation Precipitation Index (OPI) data from the NOAA series satellites. The gauge data are assembled and analyzed by the Global Precipitation Climatology Centre (GPCC) of the German Weather Service (DWD) and by the Climate Prediction Center of NOAA. The blending procedure is described in Adler et al. (2003). Here the Pentad product that provides precipitation estimates on a 2.5-degree grid over the entire globe at five-day (pentad) intervals for the period January 1979 – present (Xie et al. 2003) is used. For leap years the pentad period starting on 25 February covers six days. The data was downloaded in NetCDF format from http://www.jisao.washington.edu/data_sets/gpcp/daily/pentad.html. A comparison of GPCP with Climate Prediction Center Merged Analysis of Precipitation (CMAP) on a monthly basis revealed a good performance of GPCP data in regions with low gauge density such as West Africa (Yin et al. 2004).

For the study of some cases occurring after 1998, the Tropical Rainfall Measuring Mission (TRMM) and Other Data Precipitation Data Set (3B42 V6; Huffman et al. 2007) in a much higher spatial resolution of 0.25° is additionally used for comparison. These data are three-hourly combined microwave-IR estimates (with gauge adjustment) and were downloaded from http://disc2.nascom.nasa.gov/Giovanni/tovas/ operated by the National Aeronautics and Space Administration (NASA). The gauge data employed here are standard SYNOP observations from the archive of the DWD and the Global Summary of the Day (GSOD) data provided by the National Climatic Data Center (NCDC; ftp.ncdc.noaa.gov/pub/data/gsod/).

b. ECMWF and CLAUS data

The precipitation forecasts evaluated in this study come from the ERA-40 re-analysis project by the ECMWF (Uppala et al. 2005). Accumulated total precipitation (i.e., convective plus large-scale) from 120-hour forecasts with the ERA-40 model version T159L60 started at 0000 UTC of the first day of each of the GPCP pentads (see Section 2a) is considered, which results in a perfect temporal match. Note that this resolution is considerably coarser than the current model version T799L91. The data was retrieved from the ECMWF archive in 1°×1° lat–lon horizontal resolution and then interpolated to the GPCP 2.5°×2.5°-grid using a bicubic interpolation routine contained in the Climate Data Operators software package developed at the Max-Planck Institute for Meteorology in Hamburg (http://www.mpimet.mpg.de/fileadmin/software/cdo/). The interpolation occasionally generates spurious negative rainfalls that were set to zero.

For the analysis of the large-scale atmospheric circulation and forecast errors in Section 6 ERA-40 re-analysis and forecast fields of mean-sea level pressure (MSLP), geopotential height at 500 hPa (Z500 hereafter), and 2-m dew point temperature (TD2M hereafter) on a 1° × 1° lat–lon grid were considered that are available every six hours. Note that the TD2M fields were not directly produced by the primary 3D-Var analysis but by an optimum interpolation of measurements and are therefore comparably little influenced by the ECMWF model (see chapter 3d in Uppala et al. 2005). As a climatological background, ERA-40 long-term monthly means of 1200-UTC Z500, MSLP, and TD2M were computed for the period 1979–2001. For the analysis of clouds thermal IR window (10.5–12.5 μm) brightness temperatures (BTs) provided by the Cloud Archive User Service (CLAUS) were downloaded from the British Atmospheric Data Centre (BADC) under http://badc.nerc.ac.uk/data/claus. CLAUS merges information from several geostationary and polar-orbiting satellites (e.g., NOAA, GOES, METEOSAT, GMS) into a homogeneous global dataset (Hodges et al. 2000). The horizontal resolution of this data is 0.5° and BT fields are available every three hours for the period July 1983 to present. Unfortunately, the first four dry-seasons considered for the GPCP analysis are not covered by CLAUS, slightly reducing the numbers of cases available for the composite analysis in Section 6.

3. An example case study

As an introduction to the problem, a case study of an unusual dry-season rainfall event is presented. Figures 1a and 1b show the accumulated precipitation for the pentad 15–19 February 1999 from the GPCP and TRMM datasets together with station observations. These data clearly indicate that the precipitation zone, usually restricted to the near-equatorial Atlantic Ocean and Gulf of Guinea during the dry season (e.g., Fig. 11 in Xie and Arkin 1997), reached unusually far into the study area over the West African continent marked with black boxes in Fig. 1. The coarse-resolution GPCP data (Fig. 1a) show a maximum grid-box value in excess of 50 mm over western Nigeria and even some precipitation to the north of 10°N. The high-resolution TRMM data contain much more details and indicate regions with highest rainfalls over central Ivory Coast and western Nigeria, also with amounts exceeding 50 mm (Fig. 1b). The selected station observations confirm these unusual rainfalls, with values ranging from 46 mm at Bondoukou (8.05°N, 2.78°W) and 44 mm at Parakou (9.35°N, 2.62E) to traces as far north as Dori (14.03°N, 0.03°W). The recorded amount at Parakou corresponds to almost five times the 1961–1990 February average of 9 mm. Such amounts substantially affect the local hydrology and vegetation as exemplified in KF08. Unfortunately, the few available reports from the Nigerian synoptic network do not confirm the maxima in the satellite estimates. Interestingly, both datasets indicate scattered patches of light rain over the Sahara. The synoptic data indicates that the precipitation fell during the first four days of the pentad, mainly during the afternoon and evening hours, suggesting a triggering of convection by daytime heating. The corresponding five-day precipitation forecast from the ERA-40 data reproduces the unusual shift of the precipitation zone into the continent well, while some of the fine structure evident from the TRMM and station data is missing (Fig. 1c). This suggests that the ECMWF model is capable of simulating the changes in the large-scale circulation that allow convection to form farther north than usual, but struggles to correctly reproduce the details of the convective dynamics. Such a forecast is nevertheless of great value to the local population as discussed in the Introduction.

The unusual rainfalls are associated with a very pronounced, strongly tilted upper-level trough across northwestern Africa downstream of an equally pronounced upperridge as indicated by Z500 at 1200 UTC 17 February 1999 (Fig. 2a). MSLP is reduced over a large area to the southeast of the trough axis allowing low-level southerly moisture advection into the continent. This is clearly indicated by the northward shift of the 14°C-contour of TD2M (thick lines in Fig. 2a) that is often used as an indicator for the position of the Intertropical Discontinuity (ITD), the boundary between dry Saharan and moist tropical air over West Africa (Buckle 1996). A maximum MSLP anomaly of –8 hPa with respect to the long-term February mean is analyzed over northern Niger near 20°N, 10°E (not shown). Nine hours later CLAUS BTs show a TP along the southeastern flank of the trough (Fig. 2b). While the straight cloud band over Mali caused rather little precipitation, some rainfall was associated with the widespread deep convection over Nigeria. It is conceivable that low inertial stability at the anticyclonic flank of the subtropical jet streak accompanying the upper-trough has provided good outflow conditions for convection (Mecikalski and Tripoli 1998; Knippertz 2005). The situation resembles the dry-season precipitation case discussed in KF08, who suggested a relation between the pressure fall over West Africa and the combined affects of warm advection and an enhanced greenhouse effect under the TP. Z500, MSLP, TD2M, and CLAUS BTs will be used for the composite analysis of the dynamics of dry-season rainfalls in Section 6.

4. Climatology of dry-season precipitation events

In this section the method to obtain a climatology of dry-season precipitation events is described including an explanation of the identification algorithm and a motivation of the chosen thresholds in Section 4a. This algorithm is then applied to the entire GPCP pentad dataset in Section 4b and to the ERA-40 forecasts in Section 5. In Section 4c some remarkable events identified with the algorithm will be discussed.

a. Identification

The first step of the identification procedure is to calculate area averages of precipitation over the box indicated in Figs. 1 and 2 spanning 7.5°N–15°N, 10°W–10°E. For the GPCP pentad data this corresponds to eight grid boxes in the zonal and three grid boxes in the meridional direction, i.e. 24 grid boxes in total. The second step is to estimate a climatological background for the computation of anomalies. In order to get a smooth annual cycle from the 23 years of GPCP data, a 3-pentad (=15-days) sliding window is used, i.e., the climatological mean for a given pentad is calculated from 69 different pentad values. The investigations are restricted to the main dry season spanning the 24 pentads from 02–06 November to 25 February–01 March. During this period precipitation rates stay below 0.7 mm day^{-1}, typical of the dry season (Fig. 3). Highest values are reached for the first pentad in early November and then precipitation rates slowly decrease to values below 0.1 mm day^{-1} from mid-December to the beginning of February followed by a rather abrupt increase to values around 0.25 mm day^{-1}. The standard deviations for these 15-day means are of the same magnitude or larger than the mean values themselves indicating substantial interannual variability.

The third step of the identification routine is to calculate anomalies with respect to the mean annual cycle shown in Fig. 3. These anomalies can be expressed in absolute numbers, i.e. in units of mm day^{-1}, or in a relative sense, i.e., in percent with respect to the pertinent climatological pentad mean. This way an anomaly of –100% corresponds to no precipitation at all, while for example an anomaly of +200% means three times the average precipitation. As an example, Fig. 4 shows the anomaly values in both absolute and relative numbers for the 24 pentads of the dry season 1998/1999. Many pentads show negative anomalies, some even close to –100% indicating basically dry pentads. The fact that the absolute anomalies decrease for a given relative anomaly towards the middle of the plot is a result of the annual cycle (Fig. 3). Only eight pentads have positive anomalies demonstrating the episodic nature of dry-season rainfalls. The most prominent are Pentad 8 with +0.26 mm day^{-1} (i.e., +187%), Pentad 14 with +0.14 mm day^{-1} (i.e., +241%), and Pentad 22 with +1.3 mm day^{-1} (i.e., +538%). Pentad 22, during which more than six times more precipitation fell than usually, is the example case presented in Section 3. The area-average accumulated rainfall during this pentad is 7.7 mm, but Figs. 1a and 1b show that locally, amounts on the order of 50 mm and more were observed. The last step is the definition of a significant dry-season wet event. The identification threshold was arbitrarily set to +200% (i.e., three times the mean rainfall). In Fig. 4 only the two pentads 06–10 January and 15–19 February 1999 fulfill this criterion. A relative anomaly threshold is preferred to an absolute one to account for the annual cycle. In addition a stronger tropical influence on precipitation is expected in November and therefore the authors prefer to consider only the strongest events in this month, for which an influence of the extratropical circulation can be assumed. The obvious disadvantage of this approach is that the impact on the hydrology can differ for a typical January compared to a typical November event.

b. Climatology

When applying the +200% anomaly criterion to the 23 dry seasons 1979/80 to 2001/02, in total 43 wet events are obtained, i.e., 1.87 per year. In other words 7.8% of all pentads or about every 13th pentad is wet. Figure 5 shows a time series of the number of wet pentads per season, which varies between zero in 1982/83, 1994/95, and 2000/01 and five in 1979/80 and 1990/91. There are seven years with, respectively, one and two events. There is no obvious trend in this time series. Table 1 shows the average monthly distribution of wet events. Here a ‘month’ consists of six pentads regardless of the actual length of the calendar month (second column of Table 1). With 13 events each, most events occur in DEC and JAN, when the mean precipitation and therefore the absolute exceedance thresholds are lowest. However, the fact that there are substantially more events in the relatively wet NOV than in FEB indicates that the number of wet events in this relative sense is not simply anti-correlated with the absolute value of the exceedance threshold. Possibly, the substantial differences in soil moisture and vegetation at the beginning and end of the dry season affect inter alia vertical stability and moisture availability. The number of identified events is, of course, sensitive to the arbitrarily chosen threshold. With +300% instead of +200% the total number is reduced to only 24 events with a slightly flatter annual cycle (Table 1).

Figure 6 shows a composite of GPCP precipitation for all 43 identified dry-season wet events. Highest absolute values occur in the Atlantic ITCZ and close to southern Italy. Within the study region (marked by a black box in Fig. 6), there is a distinct south–north decrease in rainfall, but also a west–east gradient, leading to a precipitation maximum over the Guinean Highlands and leaving the five grid boxes over northern

Burkina Faso and southern Niger almost dry. Therefore restricting the study region to the southern two rows of grid boxes spanning 7.5–12.5°N would not have a very large affect on the event detection (not shown). There are five cases in which restricting the domain will increase the anomaly from just below the threshold of +200% to just above it. On the other hand there are three cases, in which rainfalls between 12.5°N and 15°N contribute substantial amounts to the area average, most notably during the pentad 21–25 January 1992, when a large precipitation band reached all across the Sahara into the Sahel. Over the entire time period the correlation between precipitation over the whole region and just the southern two rows of grid boxes is greater than 0.99. Interestingly, the composite in Fig. 6 indicates both a northward extension of the tropical precipitation zone and a southward extension of the subtropical rainfalls affecting large parts of the western and northern Sahara. This pattern is consistent with the case shown in Fig. 1 and the one analyzed by KF08, and corroborates a dynamical linkage between remote wintertime precipitation events to the south and north of the Sahara.

c. Remarkable events

The algorithm presented above identifies five events with anomalies of more than 1000%, all during the driest months DEC and JAN. These include 27–31 December 1989, 01–05 January 2000, and 06–10 January 2002. In the former two cases, the available station reports indicate widespread, moderate to abundant rainfall amounts between 10 and 47 mm in the west-central part of the study region. The latter event brought also record-breaking precipitation in excess of 50 mm to parts of Senegal and Mauritania with harmful impacts on the local population (Knippertz and Martin 2005;

Fall et al. 2007; Meier and Knippertz 2009). Station reports in the investigation area during this event peaked at 23 mm in Bouake (7.73°N, 5.06°W) and at 20 mm in Save (8.03°N, 2.48°E). Very unusual is also the 3-pentad period 12–27 December 1990 with positive anomalies of 1082%, 212%, and 1482% corresponding to an accumulated area-averaged precipitation of 12.7 mm (almost four times the DEC average, see Table 1). At Bondoukou (8.05°N, 5.06°W) the December sum of 54 mm constitutes more than four times the 1961-1990 Clino rainfall normal of 11 mm. This event is related to a repeated regeneration of a distinct trough over northern Africa. There are five more events with anomalies of more than +500%, one of which is the case presented in Section 3. The others are 16–20 January 1980, 15–19 February 1982, 21–25 January 1992, and 10–14 February 1996. In January 1980, 81 mm fell at Bondoukou (8.05°N, 5.06°W), which constitutes about ten times the average January rainfall of the 1961–1990 period. Bouake (7.73°N, 5.06°W) recorded 87 mm in February 1982. As shown in Knippertz and Martin (2005), and KF08 for January, values in excess of 100 mm per event are possible that cause local flooding at the peak of the dry season.

5. Forecast evaluation

a. Climatology

In this part the GPCP results from Section 4 are compared to five-day ERA-40 forecasts. For an optimal comparison, the exact same 23 years and 24 pentads per year (i.e., 552 pentads) are regarded with forecasts being started at 0000 UTC on the first day of the respective pentad. After applying the area average and the 3-pentad-running-window time average described in Section 4a to the forecast data, a mean seasonal cycle analogous to Fig. 3 is obtained (black bars in Fig. 7). The gray bars in Fig. 7 show the difference to GPCP in % indicating a marked wet bias of the ECMWF model with only one pentad showing an underestimation (cf. Fig. 6 in Hagemann et al. 2005). Absolute differences can be as high as 0.29 mm day^{-1} with an average over all 24 pentads of 0.08 mm day^{-1} (not shown). In a relative sense the overestimation varies from –1% to 89% with largest values in JAN and an average of 40% (Fig. 7).

Despite this wet bias the temporal accordance between the two datasets is rather good. Figure 8 shows scatter plots relating the area-averaged and grid box maximum precipitation amounts of all 552 pentads from GPCP and ERA-40. The area averages in both datasets cover the range from 0 to ~3.2 mm day^{-1} and most data points are relatively close to the diagonal without any extreme outliers (Fig. 8a). In accordance with Fig. 7, there is a general tendency of slightly higher ERA-40 values. The linear correlation coefficient r equals 0.77 indicating that the ECMWF model is able to predict more than half of the variability in this parameter. Since the data do not have a Gaussian distribution, a rank correlation is performed that basically confirms this positive result (Fig. 8b). The data points scatter uniformly around the diagonal with similar numbers of occurrences of no precipitation in both datasets. The correlation coefficient of 0.75 is only slightly lower than in Fig. 8a. For grid box maxima the correspondence between the two datasets is satisfactory as well (Fig. 8c). Both datasets span the range between zero and ~15 mm day^{-1} and again extreme outliers are rare, even for large rainfall amounts. The linear correlation coefficient still reaches 0.59 for this parameter.

b. Events

In order to examine the ability of the ECMWF model to reproduce dry-season wet events, the routine described in Section 4a was applied to ERA-40 forecasts for the same 552 pentads. Due to the positive bias found in Section 5a, the employed identification threshold corresponds to a +200% anomaly with respect to the ERA-40 forecasts and not with respect to the GPCP data. This limits the comparability between the two datasets in an absolute sense, but is unavoidable in order to obtain similar numbers of events. A sensitivity test using the GPCP thresholds resulted in an undesirable almost doubling of wet events and 3.5 times more false alarms. Using the ERA-40 thresholds, the total number of wet events in the forecasts is 34 and thus significantly smaller than in the GPCP data. This result reflects the often-documented tendency of NWP models to generate too much light precipitation while missing out on higher intensities (e.g., Frei et al. 2003). The seasonal distribution is similar to GPCP with most events in JAN (11) and DEC (9), and lesser events in NOV (6) and FEB (8) (for a definition of the periods and the corresponding GPCP results, see Table 1). The latter number indicates a tendency to overpredict FEB events. The number of events per season varies between zero (6 years) and six events in 1990/91 (not shown). The linear correlation with the GPCP time series in Fig. 5 is 0.64. There is no obvious trend or clustering of events, suggesting that changes in data availability during the ERA-40 period did not have significant impacts.

Table 2 shows an evaluation of the ERA-40 forecasts of wet events based upon the number of hits (*h*), misses (*m*), false alarms (*f*), and correct negatives (*z*) for the whole study period and two subperiods, i.e., the first eleven and the last twelve years. The first two columns indicate that 23 out of the 43 events identified in Section 4 are correctly forecasted resulting in a Hit Rate (*H*) of 0.53 (for a definition of score indices, see caption of Table 2). Eleven out of the 34 events in the ERA-40 forecasts did not verify in GPCP data, leading to a False Alarm Rate (*F*) of 0.02 and a False Alarm Ratio (*FAR*) of 0.32. *F* is the proportion of non-occurrences that were incorrectly forecasted, whereas *FAR* is the proportion of forecasts of occurrence that did not verify. For a rare event like a dry-season rainfall, *FAR* is of larger interest for an operational application. Too few events in ERA-40 forecasts result in a Frequency Bias (*B*) of 0.79. A substantially larger *H* than *F* and a Heidke Skill Score (*HSS*) of 0.56 (a *HSS* of zero means no skill and a *HSS* of one a perfect forecast) indicate a moderate skill of the ERA-40 forecasts. *H* and *FAR* vary rather little over the four months under consideration with an exception of FEB when *FAR* reaches 0.63 (not shown). Consistently FEB is the only month for which more events are predicted than observed (*B* of 1.33). In contrast, a relatively high *m* and a low *B* of 0.55 characterize NOV. When using a threshold of 300% as in Table 1, *H* and *HSS* decrease to 0.46 and 0.48, respectively, while *FAR* increases to 0.45 (not shown).

Comparing the two right-hand-side columns of Table 2 indicates an improvement in forecast skill during the last twelve years of the study period. While *FAR* and *F* do not change much, *H* increases from 0.38 to 0.68. The latter period reveals a *HSS* of 0.66 and a “perfect” *B* of 1 (22 events in both datasets). Most likely, the increasing availability of more refined satellite information and thus better initial conditions have contributed to this improvement, although natural variations could well be responsible for this behavior as well. In a pilot study to the work presented here operational ECMWF precipitation forecasts were considered instead of ERA-40 forecasts, revealing a dramatic overprediction of wet events during the 1980s and early 1990s and an increase in skill after 1997/98 (Knippertz and Fink 2008b). This progress is presumably due to both better data availability and improvements to the model and data assimilation system, in particular the change from Optimum Interpolation to 3D-Var in 1996 and to 4D-Var techniques in 1997.

The overall satisfactory performance of the ERA-40 forecasts at the ‘extreme’ end of the precipitation distribution in a tropical region was not to be expected a priori and corroborates the speculation by KF08 that dry-season precipitation in West Africa might in fact be better predicted by state-of-the-art NWP models than the more intense summer precipitation when extratropical influences are weak. In this evaluation it should be kept in mind that the ‘truth’ represented here by GPCP data also has a certain uncertainty range in a region with spatially inhomogeneous rainfalls and observations sparsely distributed in time and space. One example that illustrates the occasional disagreement between different data sources is the case study presented in Section 3 (Figs. 1a and 1b).

c. Example cases

In this subsection example cases of hits, misses, and false alarms will be discussed. The ten most extreme positive anomalies in the GPCP data with values of more than +500% (see Section 4c) are all correctly identified as wet events by ERA-40, even though anomalies are mostly not as high as in the observations. In particular the example case described in Section 3, the extreme event in January 2002 discussed among others by Knippertz and Martin (2005), and the series of three wet events in December 1990 are well reproduced. Most of the 20 misses have anomalies rather close to the required +200% in the ERA-40 forecast data, but there are also six major forecast busts with negative precipitation anomalies. These cases occur in the driest part of the year between 02 December and 04 February (Fig. 3). Absolute numbers range from 0.2–0.8 mm day^{-1} in GPCP and from 0.03–0.13 mm day^{-1} in the corresponding ERA-40 data. The most extreme case is the pentad 02–06 December 1997, when GPCP shows an anomaly of +432% with widespread precipitation over Nigeria and Benin (Fig. 9a), while ERA-40 forecasts concentrate precipitation over the western Gulf of Guinea (Fig. 9b) associated with an anomaly of -86% in the study area. For this period there is no station data available to confirm the precipitation in the southeastern part of the study region. The fact that the large-scale situation is characterized by an upper-level trough over northwestern Africa, reduced MSLP over the western Sahara accompanied by a slight northward shift of low-level moisture over the western part of the study region only (Fig. 9c), and a TP reaching from Ivory Coast to the eastern Mediterranean (Fig. 9d) casts the GPCP estimates into some doubt. A similar situation with anomalies of +295% and -88%, respectively, occurs during 26–30 January 1981.

The worst false alarm occurs during 06–10 January 1997, when ERA-40 forecasts an anomaly of more than +400%, while the GPCP indicates no precipitation at all (i.e., anomaly of -100%). All available observations show rainfalls being largely restricted to the Gulf of Guinea (Fig. 10a), while the ECMWF model shifts the rain inland over almost the entire width of the study area (Fig. 10b). The observed absence of precipitation is consistent with comparably weak troughs in the subtropics (Fig. 10c) and few clouds over the study region (Fig. 10d). The analyzed low-level moisture field, however, does show a northward shift, indicating that the model is either too moist or triggers precipitation too easily. Similar patterns are responsible for the misforecasts during 05–09 February 1986 and 07–11 December 1988, while the false alarm of 16–20 January 1996 reveals a too strong penetration only in the western half of the domain. This analysis suggests that the overprediction of rainfall in the false alarm cases in the ECMWF model is not the result of one or two unrealistic ‘grid point storms’ but rather due to regional scale problems.

6. Dynamics

In this section the dynamics of the wet events identified and investigated in the previous sections will be examined with a focus on three issues: (A) How closely does the typical evolution of a wet event agree with the case-study results by KF08 (see Introduction)? This question is addressed in subsection 6a on the basis of composites of ERA-40 re-analysis fields and CLAUS BTs for all 43 events. (B) To what extent do details of the dynamics influence the quality of the ERA-40 precipitation forecasts? This question is addressed by splitting the composites discussed in subsection 6a into hits, misses, and false alarms (subsection 6b). (C) Are cases of misforecasts related to problems with predicting the synoptic-scale setting and/or problems with the meso-scale precipitation generation? This question is addressed with composites of differences between ERA-40 60-h forecasts and corresponding ERA-40 re-analysis fields (subsection 6c). Some results in this section are illustrated with short discussions of exemplary cases.

a. The typical evolution of a wet event

For all 43 wet events Fig. 11 shows composite evolutions in Z500, MSLP, TD2M, and CLAUS BTs for DAY-8, DAY-5, DAY-2, and DAY+1 with DAY0 being the center of the pentad. Displayed are anomalies in the ERA-40 re-analysis fields with respect to long-term monthly means. Only 12 UTC values of Z500, MSLP, and TD2M were considered, while the full three-hourly resolution was used for the BT composites. Already six days before the beginning of the precipitation pentad, i.e. on DAY-8, a marked signal in both Z500 and MSLP is found (Fig. 11a). The Z500 field shows a tripole with positive anomalies to the northwest of the British Isles, negative values stretching from northwestern Africa to Russia, and finally a weakly positive anomaly centered over the Libyan coast. The negative anomaly has a structure consistent with the upper-trough shown in Fig. 2a. An inspection of the 43 single cases reveals that despite the rather strong signal the spread between individual members is large with 13 cases even having positive anomalies over northwestern Africa (not shown). The MSLP signal indicates a largely barotropic structure with negative anomalies of more than 5 hPa over the Mediterranean Sea. The area with reduced MSLP stretches as far south as northern Nigeria with only weak impacts on the low-level moisture field at this stage. The CLAUS BT anomalies (Fig. 11b) are positive to the southwest of the upper-trough, where subsidence and cloud breakup is expected, and negative to the southeast, where TP occurrence is expected (cf. Fig. 2b). McGuirk and Ulsh (1990) already documented such dry–wet dipoles in connection with TPs. Unusually cold cloud tops are also found in the area of largest negative Z500 anomalies and over the Gulf of Guinea, the Guinea Coast, and the southern part of the study area suggesting anomalous rainfall related to the reduced MSLP and marginally enhanced moisture over the continent.

Over the next three days the upper-trough and surface low move eastward to the Ionian Sea, while a new barotropic disturbance approaches northwest Africa from the west (Fig. 11c). Together the two disturbances create a region of negative MSLP anomalies covering almost entire North Africa from the Mediterranean coast to the Sahel. This allows the ITD to move northwards as indicated by the positive TD2M anomalies over the study region. The lowest absolute MSLP in the Tropics is now farther to the east (not shown) and precipitation appears to be enhanced over Cameroon and the Central African Republic (Fig. 11d). There are also anomalously cold cloud tops over the Algerian and Tunisian Atlas, to the east of the western MSLP anomaly.

Another three days later, on DAY-2, the eastern disturbance has decayed while the western disturbance has slightly shifted southward into Africa (Fig. 11e). The positive anomalies over northern Europe found throughout the entire period are strongest, creating a pronounced north–south dipole with a strong gradient between the two centers. Z500 anomalies of -5 gpm are found over the Gulf of Guinea, while MSLP is reduced by up to 2 hPa at the northern end of the study area. This situation allows moist southerlies to penetrate into the box marked in Fig. 11, as indicated by TD2M anomalies as high as 7°C (Fig. 11e). This increase in moisture feeds the unusual dry-season precipitation over the next four days. The low Z500 over the Tropics indicates a reduced vertical stability that also favors deep convection. This is consistent with the widespread negative BT anomalies reaching from the Gulf of Guinea far into the study area, particularly over Nigeria (Fig. 11f). Finally by DAY+1 the disturbance over northwest Africa has begun to weaken and to move northeastward (Fig. 11g). Interestingly, the anomaly pattern resembles DAY-8 with a weaker disturbance over the Mediterranean Sea (Fig. 11a). The TD2M and BT anomaly patterns, however, strongly differ in magnitude with anomalous low-level moisture and very cold cloud tops over the study region, a clear TP centered over Libya, and warm anomalies over Mauritania and the adjacent Atlantic (Fig. 11h).

These differences suggest that it is not the strength of the extratropical disturbance alone that matters for the tropical rainfall enhancement, but the whole evolution with a previous disturbance pre-conditioning the Tropics through poleward moisture transports as discussed by Knippertz and Martin (2005). After DAY+2 the extratropical disturbance rapidly weakens (not shown).

This composite analysis corroborates a connection between dry-season wet events in tropical West Africa with extratropical disturbances penetrating to very low latitudes. The strong signal in Z500 and MSLP almost a week before the unusual precipitation event is remarkable and suggests an importance of a succession of two extratropical disturbances. The rather weak indications of a TP during DAY-8 to DAY-2 (Figs. 11b, 11d, and 11f) suggest that in a statistical sense, the diabatic mechanism of pressure reduction found by KF08 is probably less important than its dynamic counterpart related to warm advection. The stronger TP signals for DAY-1 (not shown), DAY0 (Fig. 12b) and DAY+1 (Fig. 11h) point to a possible importance for later stages of the evolution.

b. Influence of the dynamics on the quality of the precipitation forecast

In Figs. 12a and 12b the same composites as in Fig. 11 are shown for DAY0. They largely resemble the ones for DAY+1 (Figs. 11g and 11h) but with a more pronounced TP and even colder cloud tops over the study area. If these results are now compared to corresponding composites for hits only, much more widespread cold cloud tops and higher low-level moisture are found in the study region, together with a somewhat stronger upper-level trough and a much clearer warm–cold dipole in the BT anomalies, i.e. a much clearer TP, while the MSLP signal is very similar (Figs. 12c and

12d). This suggests that events with a large-scale organization and a clear link to the extratropics are reliably reproduced. Composites for all misses have a markedly different structure. The Z500 and MSLP signals show two barotropic disturbances, one to the west of the Iberian Peninsula, and one over Tunisia and the Golf of Gabes (Fig. 12e) that do not reach as far into the Tropics as for the hits and therefore cause a weaker northward moisture advection as evident from the smaller TD2M anomalies (cp. Fig. 12c with Fig. 12e). Negative BT anomalies are analyzed to the east of the two disturbance centers and a TP stretches along their southern flanks from off the Senegalese coast to eastern Libya (Fig. 12f). In the study region there are scattered localized negative BT anomalies, but the signal is comparably weak and has no evident connection to the extratropics. This result appears consistent with frequent forecast misses in NOV (see Section 5b).

These results can be illustrated with the forecast miss 31 January – 04 February 1998. At 1200 UTC 02 February the Z500 and MSLP distributions (Fig. 13a) show a strong disturbance to the west of the Iberian Peninsula and a weak trough over the eastern Mediterranean consistent with the composite in Fig. 12e. Negative MSLP anomalies are found over entire northern Africa down to about 12°N (not shown) that are associated with enhanced moisture transports into the continent (Fig. 13a). The upper-trough, however, is too remote to directly influence the precipitation generation as for example during the case in February 1999 (Fig. 2a). Instead, CLAUS BT data for this period indicate precipitation generation by rather localized convective cells forming in the afternoon hours of 31 January, and 01 and 02 February (Figs. 13b and 13c). In the GPCP data the precipitation zone penetrates into the eastern and central part of the study region, consistent with the CLAUS data and the few available station observations (Fig. 13d), leading to an area-averaged anomaly of 398%. The TRMM data shows more localized precipitation over Ghana, Togo, and Benin (Fig. 13e). The disagreement between the observational datasets underlines the general difficulty of forecast evaluation in this region discussed earlier in this paper. The ERA-40 forecasts extend the precipitation zone into the study region, but not widespread and not intense enough (Fig. 13f), resulting in an area-averaged anomaly of -23%. These results suggest difficulties of the ECMWF model to trigger convection in cases with an anomalous moisture inflow into the study region prior to DAY0 but without a direct synoptic forcing by an upper-level trough as for the hits. The possible influence of a misforecasted synoptic setting is addressed in subsection 6c.

The composite analysis for the false alarm cases reveals very large anomalies in Z500, MSLP, and TD2M (Fig. 12g). Note, however, that the strength of the anomalies is strictly speaking not directly comparable to the hits and misses due to the smaller sample size. In contrast to the other cases the orientation of the Z500 anomaly is from northwest to southeast, leading to negative vorticity advection, subsidence, and positive BT anomalies over large parts of West Africa (Fig. 12h). The MSLP shows strongest anomalies over the Bay of Biscay (< -5 hPa) and over northeastern Niger (< -4 hPa). The latter is associated with enhanced moisture inflow into the continent as reflected in large positive TD2M anomalies (Fig. 12g), while substantial cold BT anomalies are restricted to the southeastern corner of the study area (Fig. 12h). Possibly the strong subsidence creates a rather dry and stable mid-troposphere with capping inversions, which is not conducive for deep convection, even in the presence of low-level most air. It is conceivable that the ECMWF model struggles to capture such stable layers and therefore forecasts too much precipitation in these situations. A thorough investigation of this idea would require a detailed comparison with available radiosonde data, which is beyond the scope of this paper. Possible other reasons are an underestimation of precipitation in the GPCP data, for example, due to a lack of surface observations or a mispredicted synoptic setting. The first hypothesis cannot be tested without an additional independent source of information to evaluate the GPCP data. The second will be addressed in the next subsection.

c. Predictions of the synoptic setting

For this analysis, ERA-40 forecasts of Z500, MSLP, and TD2M started at 0000 UTC of DAY-2 of the respective pentad and then run for 60 hours until 1200 UTC on DAY0 are compared to the corresponding ERA-40 re-analyses in the form of composites for all events, all hits, all misses, and all false alarms as in Fig. 12. For all wet events the ERA-40 forecasts reveal a positive MSLP and Z500 bias over the western Mediterranean Sea and adjacent North Africa (Fig. 14a), indicating a somewhat too weak disturbance in the forecast (cf. Fig. 12a). In the Tropics, Z500 and MSLP are systematically forecasted too low, consistent with a too high TD2M over the study region. If the composite is split into hits and misses, the forecast errors with respect to the large-scale circulation do not change significantly (Figs. 14b and 14c). Both hits and misses show a wet bias over the study region with the one for misses being somewhat smaller, which might explain part of why the model generates too little precipitation in these cases. The differences in the Z500 errors over the study region are presumably too small to have a substantial impact, although the positive values for the misses are at least consistent with less precipitation.

The forecast errors for false alarms have a different structure and are of larger magnitude (Fig. 14d), which again may be due to the smaller number of composite members. The most prominent signals are a TD2M error in the study region of as much as 10°C, a large northwest–southeast oriented region with positive deviations in Z500 and MSLP stretching from the Atlantic into northwest Africa, and a region with negative values over the central Mediterranean Sea and adjacent parts of Europe. This indicates a reduction of the negative trough orientation evident from Fig. 12g in the model, which would reduce the subsidence to the southwest and south of the trough with potential positive effects on precipitation. In the Tropics, however, the signals in Z500 and MSLP do not differ much from the result for all events (Fig. 14a), pointing to a rather indirect effect of these forecast errors.

To illustrate this further, Fig. 15 shows the false alarm example of 15–19 February 1991. For this period GPCP data and station observations indicate an unusual penetration of rainfalls into the study area but with rather low amounts (Fig. 15a), while the ERA-40 model forecasts more widespread and more intense rainfalls (Fig. 15b). The synoptic situation on DAY0 of the pentad is characterized by a conspicuous disturbance close to the Iberian Peninsula connected to a low-pressure corridor stretching from Niger to Algeria that is most likely responsible for the shift of the ITD and the rain zone into the study region (Fig. 15c). These patterns closely agree with the false alarm composite shown in Fig. 12g. Consistent with Fig. 14d, the forecast errors are comparably large, reaching positive values in Z500 of more than 60 gpm over the Atlantic and Algeria, and negative values of the same magnitude over the western Mediterranean Sea (Fig. 15d). Corresponding to the upper-level patterns, maximum MSLP errors are as large as +11 hPa over the Portuguese coast and -4 hPa over northeastern Spain. These errors shift the disturbance center from the western to the eastern side of the Iberian Peninsula and lead to a more positively tilt of the upper-level trough and slightly lower MSLP in a band stretching from Guinea to Libya. The latter is consistent with the positive TD2M errors and stronger precipitation in the model. Interestingly, there is also a pronounced positive TD2M error close to the border triangle Algeria–Mali–Niger (Fig. 15d). In conclusion, these results suggest that the false alarms are to some degree related to worse forecasts of the large-scale circulation, in particular of the moisture distribution in the Tropics and the orientation of the trough axis in the subtropics, which determines the vertical motion patterns. In addition, problems with the precipitation generation, specifically with the suppression of deep convection through capping inversions, and also with the quality of the observations cannot be ruled out.

7. Summary and conclusions

Precipitation events during the heart of the dry-season in tropical West Africa from November to February are rare, but can have high impacts locally. Previous work has suggested a link to upper-level troughs from the extratropics and a comparably high predictability of such events (KF08), which is potentially of great benefit to the local population. Here an identification routine for such dry-season wet events was developed based on 23 winter seasons from the GPCP merged satellite-gauge pentad dataset. The algorithm uses an area-averaged (7.5–15°N, 10°W–10°E) threshold of +200% anomaly relative to the mean seasonal cycle, resulting in an identification of 1.87 events per winter on average with a range from zero to five. Most events occur in December and January when the absolute exceedance thresholds are lowest. A composite analysis revealed that the unusual precipitation is in fact connected to distinct upper-level disturbances in the subtropics and an associated lowering of the MSLP over the Sahara that allows moist southerlies to penetrate farther than usual during this season into the continent. The analysis also points to an impact of low-level moisture inflow connected to a preconditioning prior disturbance about one week before the actual precipitation event in agreement with a case study by KF08. For extreme precipitation events in regions closer to the West African west coast Knippertz and Martin (2005) also found a preconditioning through mid-tropospheric moisture advection from the deep Tropics ahead of a precursor upper-level trough. This general behavior of a several day-long moistening of the seasonally dry troposphere may help African forecasters in their day-to-day operations to anticipate the potential for high-impact weather events as early as possible. The actual wet events are accompanied by TPs to the east of the upper-troughs and by unusual precipitation at the northern and western fringes of the Sahara as already documented by KF08. With respect to the dynamical concept developed on a case study basis by KF08 the statistical results presented here suggest that the pressure fall over the Sahara is mainly related to adiabatic warm advection to the southeast of the upper-trough and to a lesser degree by diabatic warming under the TP due to an increased greenhouse effect. The latter may be important in later stages of the evolution or in transition season cases when warm advection and vertical motions associated with the troughs are weaker.

The evaluation of five-day precipitation forecasts from the ERA-40 re-analysis dataset led to the following conclusions: (A) There is an overall wet bias in the model over the study region. (B) The temporal correlation of area averages to GPCP is highly significant with 0.77. (C) The number of wet events is underpredicted leading to a bias of 0.79 and a hit rate of 0.53 with the strongest ten events all well reproduced. (D) The false alarm ratio is only 0.32 indicating an overall moderate skill of the five-day forecasts (in contrast to many other tropical precipitation systems, e.g., Montmerle et al. 2006), which even increases in the later half of the study period. (E) Typical hits are characterized by a deep penetration of the extratropical disturbance into West Africa, a distinct TP, and a large-scale organization of convection in the Tropics through the pronounced trough. (F) Typical misses are characterized by a northward shifted moist zone without a deep penetration of extratropical disturbances. The abundance of low-level moisture favors the development of localized convective cells in the course of the day that are apparently less reliably reproduced by the ECMWF model. (G) Typical false alarms show a more negative orientation of the extratropical disturbance, strong subsidence over large parts of West Africa, and enhanced cloudiness over the eastern part of the study region. Possible reasons for the too strong precipitation in the ECMWF model forecasts are too moist low levels, problems with the suppression of deep convection through capping inversions in the subsidence zone and/or a more positively tilted trough orientation in the subtropics. These results corroborate the hypothesis of KF08 that a strong extratropical influence generally enhances the quality of predictions in the Tropics. In our view the presented results are promising enough to be taken advantage of by national weather services in West Africa.

One problem evident from this study is the, at times, questionable quality of the coarse resolution GPCP data used for forecast evaluation related to the sparse gauge network in West Africa (see Yin et al. 2004). Therefore the authors intend to repeat some of the investigations presented here with the high-resolution, high-quality TRMM data available for 1998–present. A comparison of this dataset to the state-of-the-art ERA-interim re-analysis would allow a further exploration of the impact of a more refined assimilation system on forecast improvements. Moreover spatial correlations could be considered instead of area averages to allow a more regional evaluation that is of more practical use. It would also be interesting to include extratropical influences during the post- and pre-monsoon season, i.e. during October, March, and April. Another aspect raised but not entirely clarified in this and previous studies is the mechanism of pre-conditioning by a prior disturbance. Possible hypotheses are that an enhancement of soil moisture or a moister mid-troposphere improves conditions for subsequent rainfalls.

Acknowledgments.

The authors acknowledge funding under the Emmy Noether program of the German Science Foundation (DFG; Grant KN 581/2–3) and under the IMPETUS Project (BMBF Grant 01LW06001A, North Rhine-Westphalia Grant 313-21200200). We are especially indebted to Jonas von Schumann, Volker Ermert, Sonja Eikenberg, and Yvonne Tuchscherer for their help in data acquisition, analysis, and visualization. We would like to thank Anton Beljaars for help with retrieving the ERA-40 five-day forecasts, and Heini Wernli and two anonymous reviewers for their helpful comments that substantially improved the manuscript. For the case studies Ernest Afiesimama from the Nigerian Meteorological Service NIMET and the GLOWA Volta project gratefully provided daily rainfall data from Nigeria and Ghana, respectively. Athanase Bizimana from ACMAD kindly furnished us with the 1961–1990 CLINO values for some stations in Ivory Coast.

References

Adler, R. F., G. J. Huffman, A. Chang, R. Ferraro, P. Xie, J. Janowiak, B. Rudolf, U. Schneider, S. Curtis, D. Bolvin, A. Gruber, J. Susskind, and P. Arkin, 2003: The Version 2 Global Precipitation Climatology Project (GPCP) monthly precipitation analysis (1979–present). *J. Hydrometeor.*, **4,** 1147–1167.

Borgne, J. L., 1979: Un exemple d'invasion polaire sur la région mauritano-sénégalaise. *Ann. Géograph.,* **489,** 521–548.

Buckle, C., 1996: *Weather and climate in Africa*. Longman, Harlow, UK, 312 pp.

Dubief, J., and P. Queney, 1935: Les grands traits du climat du Sahara algérien. *La Météorologie*, 81–91.

Fall, S., D. Niyogi, U. C. Mohanty, and A. Kumar, 2007: Application of weather prediction models for hazard mitigation planning: A case study of heavy off-season rains in Senegal. *Nat. Hazards,* **41,** 227–243.

Frei, C., J. H. Christensen, M. Déqué, D. Jacob, R. G. Jones, and P. L. Vidale, 2003: Daily precipitation statistics in regional climate models: Evaluation and intercomparison for the European Alps. *J. Geophys. Res.,* **108(D3),** 4124, doi:10.1029/2002JD002287.

Gaye, A. T., S. Fongang, A. Garba, and D. Badiane, 1994: Study of Heug rainfall in Senegal using conventional data and Meteosat imagery. Veille Climatique Satellitaire, Lannion, France, Ministère de la Coopération - ORSTOM - METEO-FRANCE, 61–71.

Griffiths, J. F., 1972: Semi-arid zones. *World Survey of Climatology*, H. E. Landsberg, Ed., Elsevier, pp. 193–210.

Hagemann, S., K. Arpe, and L. Bengtsson, 2005: *Validation of the hydrological cycle of ERA-40*. ERA-40 Project Report Series No. 24, 42pp.

Hodges, K., D. W. Chappell, G. J. Robinson, and G. Yang, 2000: An improved algorithm for generating global window brightness temperatures from multiple satellite infra-red imagery. *J. Atmos. Ocean Tech.,* **17,** 1296–1312.

Huffman, G. J., R. F. Adler, S. Curtis, D. T. Bolvin, and E. J. Nelkin, 2007: Global rainfall analyses at monthly and 3-hr time scales. *Measuring precipitation from space: EURAINSAT and the future*, V. Levizzani, P. Bauer, F. J. Turk, Eds., Springer Verlag (Kluwer Academic Publishers), Dordrecht, chapter 23, pp. 291–306.

Issar, A. S., 1995: *Impacts of climate variations on water management and related socio-economic systems*. Technical Documents in Hydrology, International Hydrological Programme, UNESCO, Paris, 97pp.

Kållberg, P., P. Berrisford, B. Hoskins, A. Simmons, S. Uppala, S. Lamy-Thépaut, and R. Hine, 2005: *ERA-40 atlas*. ERA-40 Project Report Series, 19, ECMWF, Shinfield Park, Reading, UK, 191 pp.

Knippertz, P., 2005: Tropical–extratropical interactions associated with an Atlantic tropical plume and subtropical jet streak. *Mon. Wea. Rev.*, **133,** 2759–2776.

——, and J. E. Martin, 2005: Tropical plumes and extreme precipitation in subtropical and tropical West Africa. *Quart. J. Roy. Meteor. Soc.*, **131,** 2337–2365.

——, and A. H. Fink, 2008a: Dry-season precipitation in tropical West Africa and its relation to forcing from the extratropics. *Mon. Wea. Rev.*, **136 (9),** 3579–3596.

——, and ——, 2008b: Rainfall events during the West African dry-season: Forcing from the extratropics and predictability. AMS Conference on Hurricanes and Tropical Meteorology, Orlando, FL, April 2008. AMS, Boston.

Leroux, M., 2001: *The meteorology and climate of tropical Africa*. Springer, 493 pp.

Mason, I. B., 2003: Binary events. Chapter 3 in: Jolliffe, I. T. and D. B. Stephenson, Eds., *Forecast verification. A practitioner's guide in atmospheric science*. Wiley, Chichester, UK.

Meier, F., and P. Knippertz, 2009: Dynamics and predictability of a heavy dry-season precipitation event over West Africa – Sensitivity experiments with a global model. *Mon. Wea. Rev.*, **137(1),** 189–206.

McGuirk, J. P., and D. J. Ulsh, 1990: Evolution of tropical plumes in VAS water vapor imagery. *Mon. Wea. Rev.*, **118,** 1758–1766.

Mecikalski, J. R., and G. J. Tripoli, 1998: Inertial available kinetic energy and the dynamics of tropical plume formation. *Mon. Wea. Rev.*, **126,** 2200–2216.

Montmerle, T., J.-P. Lafore, L. Berre, and C. Fischer, 2006: Limited- area model error statistics over Western Africa: Comparisons with midlatitude results. *Quart. J. Roy. Meteor. Soc.*, **132,** 213–230.

Seck, A., 1962: Le Heug ou pluies de saison sèche au Sénégal. *Ann. Géograph.*, **385,** 225–246.

Uppala, S. M., P. W. Kållberg, A. J. Simmons, U. Andrae, V. da Costa Bechtold, M. Fiorino, J. K. Gibson, J. Haseler, A. Hernandez, G. A. Kelly, X. Li, K. Onogi, S. Saarinen, N. Sokka, R. P. Allan, E. Andersson, K. Arpe, M. A. Balmaseda, A. C. M. Beljaars, L. van de Berg, J. Bidlot, N. Bormann, S. Caires, F. Chevallier, A. Dethof,

M. Dragosavac, M. Fisher, M. Fuentes, S. Hagemann, E. Hólm, B. J. Hoskins, L. Isaksen, P. A. E. M. Janssen, R. Jenne, A. P. McNally, J.-F. Mahfouf, J.-J. Morcrette, N. A. Rayner, R. W. Saunders, P. Simon, A. Sterl, K. E. Trenberth, A. Untch, D. Vasiljevic, P. Viterbo, and J. Woollen, 2005: The ERA-40 re-analysis. *Quart. J. Roy. Meteor. Soc.*, **131,** 2961–3012.

Xie, P., and P. A. Arkin, 1997: Global precipitation: A 17-year monthly analysis based on gauge observations, satellite estimates, and numerical model outputs. *Bull. Amer. Meteorol. Soc.*, **78(11),** 2539–2558.

——, J. E. Janowiak, P. A. Arkin, R. F. Adler, A. Gruber, R. R. Ferraro, G. J. Huffman, S. Curtis, 2003: GPCP pentad precipitation analyses: An experimental dataset based on gauge observations and satellite estimates. *J. Climate,* **16,** 2197–2214.

Yin, X., A. Gruber, and P. Arkin, 2004: Comparison of the GPCP and CMAP merged gauge-satellite monthly precipitation products for the period 1979–2001. *J. Hydrometeor.*, **5,** 1207–1222.

List of Figures

FIG. 1. Five-day accumulated precipitation during the pentad 15–19 Feb. 1999 (in mm) from (a) GPCP, (b) TRMM, and (c) ERA-40 forecast data. Observations from selected rain gauges are indicated as numbers, with ‘0’ indicating traces of rain. Black boxes mark the study area.

FIG. 2. (a) Z500 (contours every 50 gpm), MSLP (shading), and 14°C contour of TD2M (thick solid line) at 1200 UTC 17 Feb. 1999. The dashed line shows the 1979–2002 February average of the latter contour as a reference. (b) CLAUS IR brightness temperatures at 2100 UTC on this day. Black boxes mark the study area.

FIG. 3. Mean pentad precipitation (in mm day^{-1}) over the area 7.5°N–15°N, 10°W–10°E during the West African dry season 02 Nov. to 01 March based upon GPCP pentad precipitation estimates of the 23 dry seasons 1979/80 to 2001/02. The dates on the abscissa give the center day of the respective pentad. Months are defined as in Table 1.

FIG. 4. Pentad precipitation anomalies over the area 7.5°N–15°N, 10°W–10°E during the West African dry season 02 Nov. 1998 to 01 March 1999. Anomalies were calculated with respect to the mean pentad values displayed in Fig. 3 and expressed in mm day^{-1} (gray bars, right ordinate) and in % (black bars, left ordinate), respectively. The dates on the abscissa give the center day of the respective pentad, which are numbered serially for reference in the text.

FIG. 5. Number of precipitation events for the 23 dry-seasons 1979/80 to 2001/02 as identified from GPCP pentad data using the routine described in Section 4a.

FIG. 6. Composited GPCP precipitation over all 43 wet events identified in Section 4 in mm per pentad. A black box marks the study area.

FIG. 7. Black bars show the mean annual cycle of precipitation as in Fig. 3 but based upon five-day ERA-40 precipitation forecasts. The gray bars indicate the difference between ERA-40 and GPCP data in %.

FIG. 8. Scatter plots relating pentad precipitation data from GPCP (abscissae) to ERA-40 five-day forecasts (ordinates) for the 552 pentads 02 Nov.–01 March 1979/80–2001/02. (a) Area averages for 7.5°N–15°N, 10°W–10°E in mm day^{-1}. (b) Ranking of the area averages shown in (a). Rank 494 in the GPCP data and rank 499 in the ERA-40 data corresponds to zero precipitation. (c) As (a) but for the 2.5° x 2.5° grid box maxima. The linear correlation coefficient *r* is given in each panel. All correlations are significant at the 99.9% significance level.

FIG. 9. Example of an extreme forecast miss. Five-day accumulated precipitation during the pentad 02–06 Dec. 1997 (in mm) from (a) ERA-40 forecast data and (b) GPCP. Only the synoptic station Odienne reported precipitation during this period. (c) CLAUS IR brightness temperatures at 2100 UTC on 04 Dec. 1997. (d) Analyzed Z500 (contours every 50 gpm), MSLP (shading), and 14°C contour of TD2M (thick solid line) at

1200 UTC 04 Dec. 1997. The dashed line shows the 1979–2001 December average of the latter contour as a reference. Black boxes mark the study area.

FIG. 10. Example of an extreme false alarm. Five-day accumulated precipitation during the pentad 06–10 Jan. 1997 (in mm) from (a) ERA-40 forecast data and (b) GPCP. Only the synoptic station Djougou reported traces of precipitation during this period. (c) CLAUS IR brightness temperatures at 2100 UTC on 07 Jan. 1997. (d) Analyzed Z500 (contours every 50 gpm), MSLP (shading), and 14°C contour of TD2M (thick solid line) at 1200 UTC 07 Jan. 1997. The dashed line shows the 1979–2002 January average of the latter contour as a reference. Black boxes mark the study area..

FIG. 11. Composited anomalies of Z500 (green contours every 5 gpm), MSLP (shaded), and TD2M (red contours showing 2, 4, and 6 °C) (left panels), as well as CLAUS IR BTs (right panels) over all 43 wet events identified in Section 4b. (a)–(b) DAY-8, (c)–(d) DAY-5, (e)–(f) DAY-2, and (g)–(h) DAY+1. No CLAUS data is available before 1983, so that these composites consist of only 35 events. Black boxes mark the study area. Note the different geographical areas in the right and left panels.

FIG. 12. Composited anomalies of analyzed Z500 (contoured every 5 gpm), MSLP (shaded), and TD2M (red contours showing 2, 4, 6, and 8 °C) (left panels), as well as CLAUS BTs (right panels) for DAY0 over (a)–(b) all 43 wet events, (c)–(d) all 23 hits, (e)–(f) all 20 misses, and (g)–(h) all 11 false alarms. No CLAUS data is available before 1983, so that these composites consist of 35 events in (b), 20 events in (d), and 15 events

in (f). The false alarms are not affected. Black boxes mark the study area. Note the different geographical areas in the right and left panels.

FIG. 13. Example of a forecast miss. (a) Analyzed Z500 (contours every 50 gpm), MSLP (shading), and 14°C contour of TD2M (thick solid line) at 1200 UTC 02 Feb. 1998. The dashed line shows the 1979–2002 February average of the latter contour as a reference. (b)–(c) CLAUS IR brightness temperatures at 2100 UTC on 01 and 02 February, respectively. (d)–(f) as Fig. 1 but for 31 Jan. – 04 Feb. 1998. Black boxes mark the study area.

FIG. 14. Composited differences of Z500 (green contours every 4 gpm), MSLP (shaded), and TD2M (red contours showing 2, 4, 6, 8, and 10°C) between ERA-40 60-hour forecasts and the corresponding re-analysis for DAY 0: (a) all 43 wet events, (b) all 23 hits, (c) all 20 misses, and (d) all 11 false alarms. Black boxes mark the study area.

FIG. 15. Example of a false alarm. (a)–(b) As Figs. 1a and 1c but for 15–19 Feb. 1991. (c) Z500 (contours every 50 gpm), MSLP (shading), and 14°C contour of TD2M (red solid line) at 1200 UTC 17 Feb. 1991. The dashed red line shows the 1979–2002 February average of the latter contour as a reference. (d) Differences of Z500 (contoured every 15 gpm), MSLP (shaded), and TD2M (red contours showing 6, 10, and 14°C) between the ERA-40 60-hour forecast valid at 1200 UTC 17 Feb. 1991 and the corresponding re-analysis. Black boxes mark the study area.

TABLE 1. Monthly statistics of mean precipitation and number of dry-season precipitation events for two different thresholds. Data basis are the GPCP pentad precipitation estimates for the 23 dry seasons 1979/80 to 2001/02. For details on the identification of events, see Section 4a.

Month	Period	Mean precipitation	# wet events (> 200%)	# wet events (> 300%)
NOV	02 Nov. – 01 Dec.	0.33 mm day^{-1}	11	5
DEC	02 – 31 Dec.	0.11 mm day^{-1}	13	9
JAN	01 – 30 Jan.	0.07 mm day^{-1}	13	5
FEB	31 Jan. – 01 Mar.	0.21 mm day^{-1}	6	5
All	02 Nov. – 01 Mar.	0.18 mm day^{-1}	43	24

TABLE 2. Quality of ERA-40 forecasts of dry-season wet events evaluated with GPCP data. The rows give numbers of hits (h), misses (m), false alarms (f), correct negatives (z), and total number of dates (n) for the whole study period and two subperiods. The definition of the indices used are (see Mason 2003 for more details): Frequency Bias $B = (h+f)/(h+m)$, Hit Rate $H = h/(h+m)$, False Alarm Rate $F = f/(f+z)$, False Alarm Ratio $FAR = f/(h+f)$, and the Heidke Skill Score $HSS = (PC–E)/(1–E)$, where PC is proportion correct ($PC = (h+z)/n$) and E is the proportion of forecasts that would have been correct, if forecasts and observations were independent: $E = 1/n^2[(h+m)(h+f)+(z+m)(z+f)]$. The HSS varies between 0 (no skill) and 1 (perfect forecast).

Period	1979/80–2001/02	1979/80–1989/90	1990/91–2001/02
h	23	8	15
m	20	13	7
f	11	4	7
z	498	239	259
n	552	264	288
B	0.79	0.57	1.00
H	0.53	0.38	0.68
F	0.02	0.02	0.03
FAR	0.32	0.33	0.32
HSS	0.57	0.45	0.66

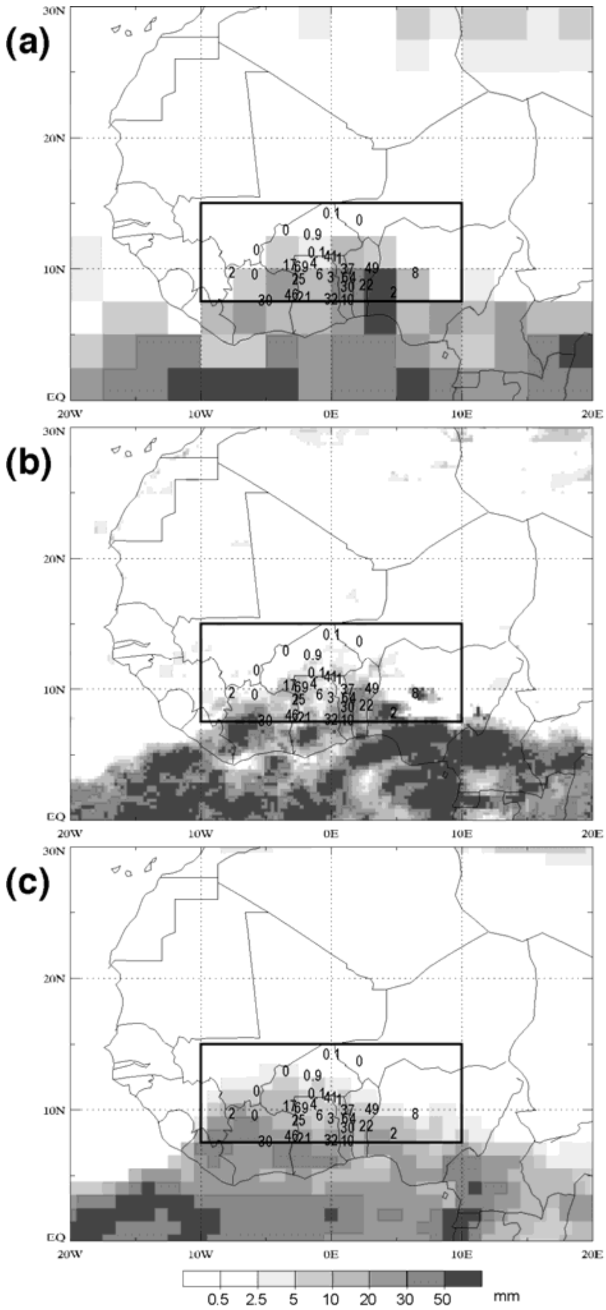

FIG. 1. Five-day accumulated precipitation during the pentad 15–19 Feb. 1999 (in mm) from (a) GPCP, (b) TRMM, and (c) ERA-40 forecast data. Observations from selected rain gauges are indicated as numbers, with '0' indicating traces of rain. Black boxes mark the study area.

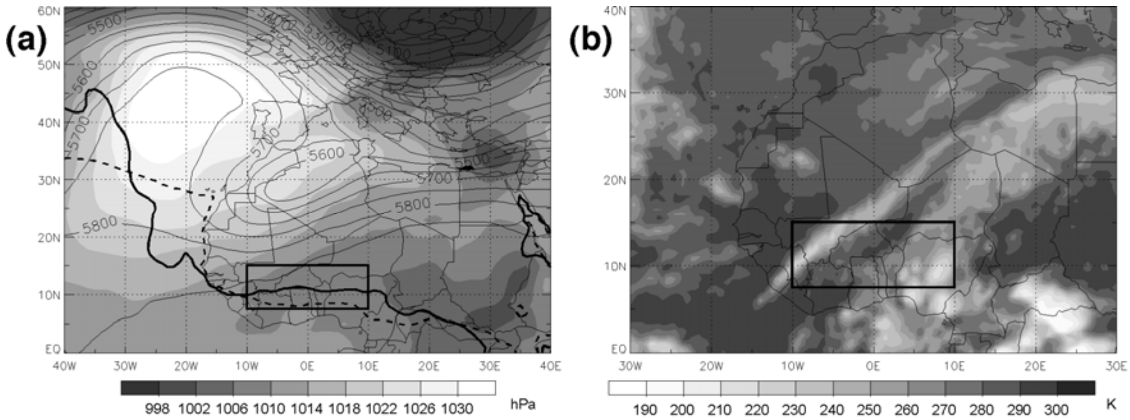

FIG. 2. (a) Z500 (contours every 50 gpm), MSLP (shading), and 14°C contour of TD2M (thick solid line) at 1200 UTC 17 Feb. 1999. The dashed line shows the 1979–2002 February average of the latter contour as a reference. (b) CLAUS IR brightness temperatures at 2100 UTC on this day. Black boxes mark the study area.

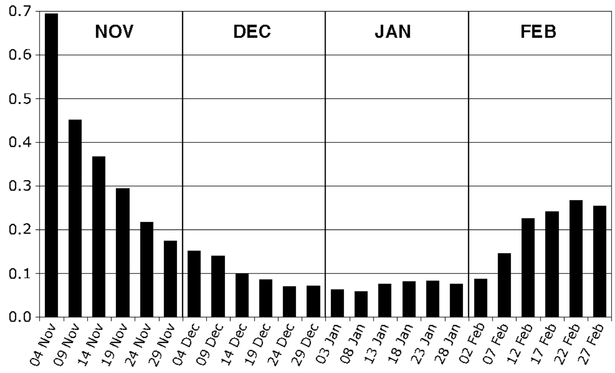

FIG. 3. Mean pentad precipitation (in mm day^{-1}) over the area 7.5°N–15°N, 10°W–10°E during the West African dry season 02 Nov. to 01 March based upon GPCP pentad precipitation estimates of the 23 dry seasons 1979/80 to 2001/02. The dates on the abscissa give the center day of the respective pentad. Months are defined as in Table 1.

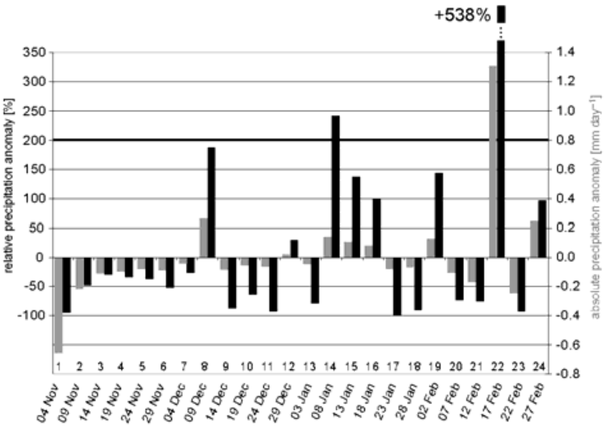

FIG. 4. Pentad precipitation anomalies over the area 7.5°N–15°N, 10°W–10°E during the West African dry season 02 Nov. 1998 to 01 March 1999. Anomalies were calculated with respect to the mean pentad values displayed in Fig. 3 and expressed in mm day^{-1} (gray bars, right ordinate) and in % (black bars, left ordinate), respectively. The dates on the abscissa give the center day of the respective pentad, which are numbered serially for reference in the text.

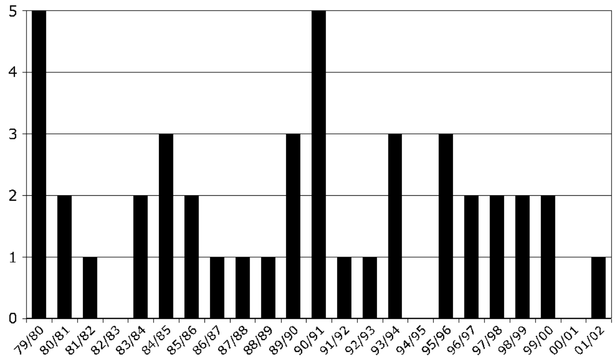

FIG. 5. Number of precipitation events for the 23 dry-seasons 1979/80 to 2001/02 as identified from GPCP pentad data using the routine described in Section 4a.

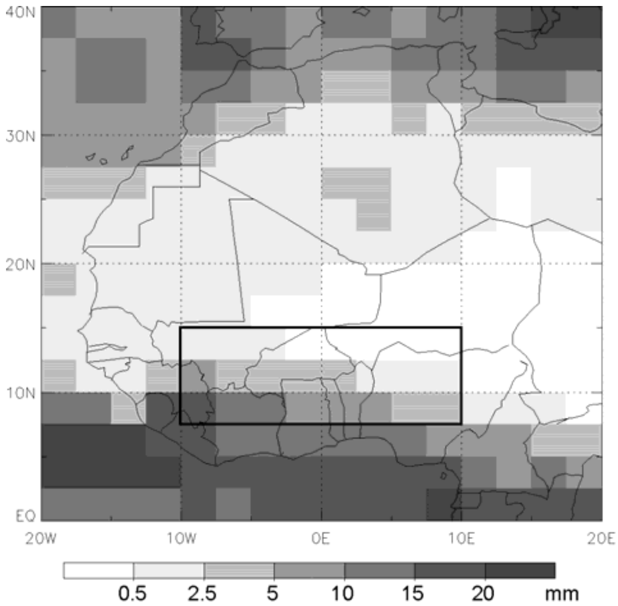

FIG. 6. Composited GPCP precipitation over all 43 wet events identified in Section 4 in mm per pentad. A black box marks the study area.

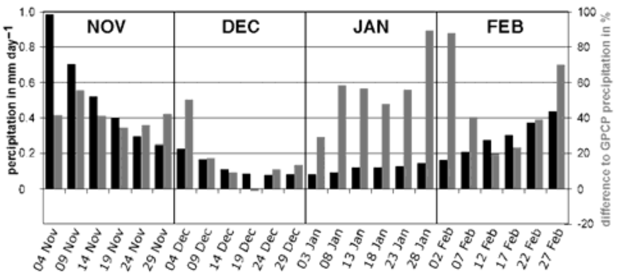

FIG. 7. Black bars show the mean annual cycle of precipitation as in Fig. 3 but based upon five-day ERA-40 precipitation forecasts. The gray bars indicate the difference between ERA-40 and GPCP data in %.

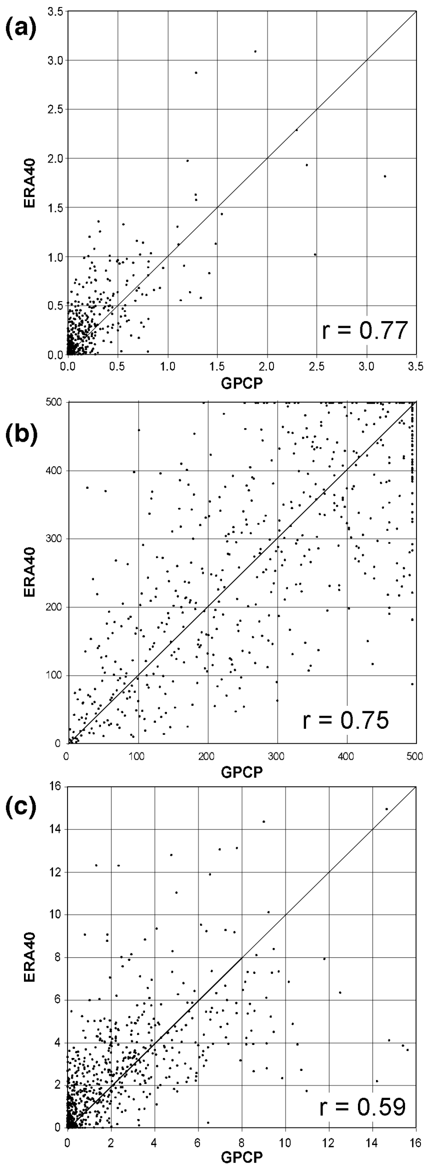

FIG. 8. Scatter plots relating pentad precipitation data from GPCP (abscissae) to ERA-40 five-day forecasts (ordinates) for the 552 pentads 02 Nov.–01 March 1979/80–2001/02. (a) Area averages for 7.5°N–15°N, 10°W–10°E in mm day^{-1}. (b) Ranking of the area averages shown in (a). Rank 494 in the GPCP data and rank 499 in the ERA-40 data corresponds to zero precipitation. (c) As (a) but for the 2.5° x 2.5° grid box maxima. The linear correlation coefficient *r* is given in each panel. All correlations are significant at the 99.9% significance level.

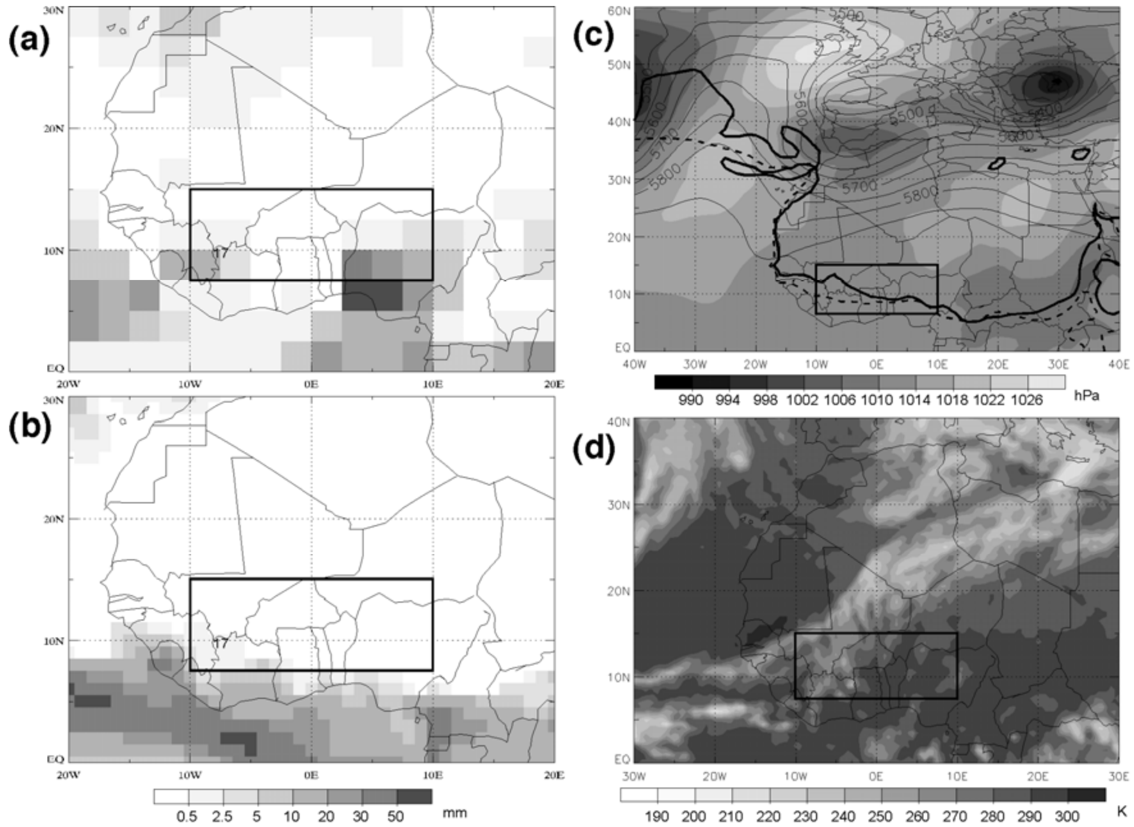

FIG. 9. Example of an extreme forecast miss. Five-day accumulated precipitation during the pentad 02–06 Dec. 1997 (in mm) from (a) ERA-40 forecast data and (b) GPCP. Only the synoptic station Odienne reported precipitation during this period. (c) CLAUS IR brightness temperatures at 2100 UTC on 04 Dec. 1997. (d) Analyzed Z500 (contours every 50 gpm), MSLP (shading), and 14°C contour of TD2M (thick solid line) at 1200 UTC 04 Dec. 1997. The dashed line shows the 1979–2001 December average of the latter contour as a reference. Black boxes mark the study area.

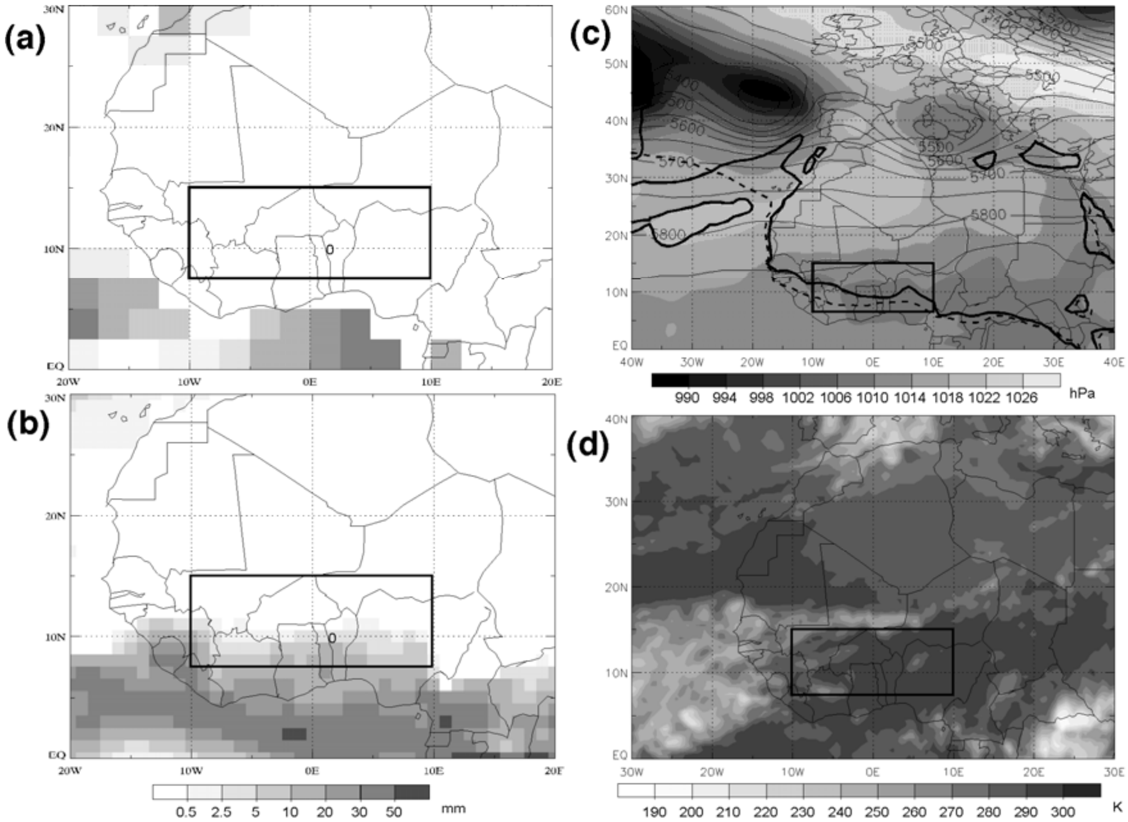

FIG. 10. Example of an extreme false alarm. Five-day accumulated precipitation during the pentad 06–10 Jan. 1997 (in mm) from (a) ERA-40 forecast data and (b) GPCP. Only the synoptic station Djougou reported traces of precipitation during this period. (c) CLAUS IR brightness temperatures at 2100 UTC on 07 Jan. 1997. (d) Analyzed Z500 (contours every 50 gpm), MSLP (shading), and 14°C contour of TD2M (thick solid line) at 1200 UTC 07 Jan. 1997. The dashed line shows the 1979–2002 January average of the latter contour as a reference. Black boxes mark the study area.

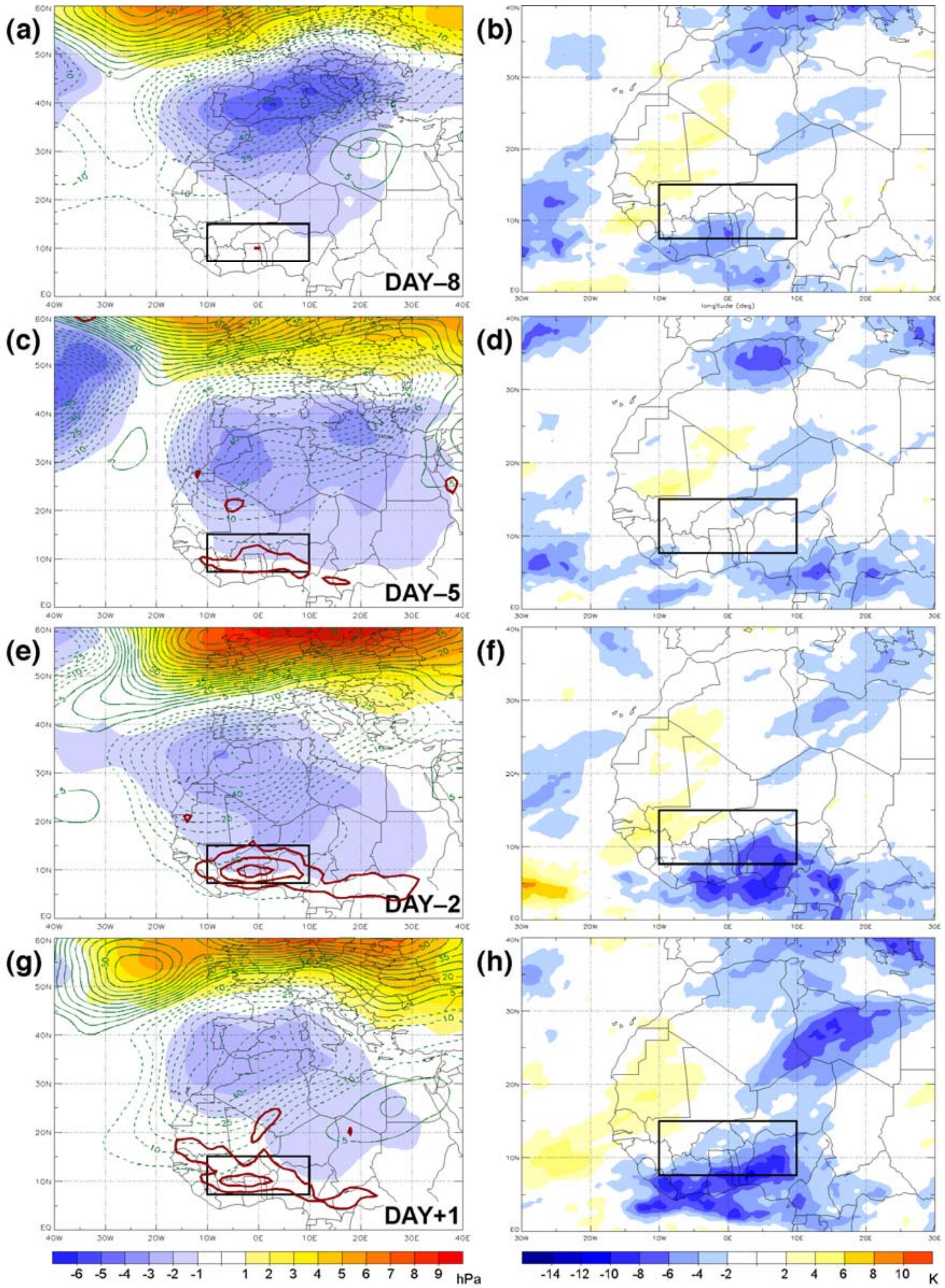

(a)
(b)
DAY–8
(c)
(d)
DAY–5
(e)
(f)
DAY–2
(g)
(h)
DAY+1
-6 -5 -4 -3 -2 -1 1 2 3 4 5 6 7 8 9 hPa
-14 -12 -10 -8 -6 -4 -2 2 4 6 8 10 K

FIG. 11. Composited anomalies of Z500 (green contours every 5 gpm), MSLP (shaded), and TD2M (red contours showing 2, 4, and 6 °C) (left panels), as well as CLAUS IR BTs (right panels) over all 43 wet events identified in Section 4b. (a)–(b) DAY-8, (c)–(d) DAY-5, (e)–(f) DAY-2, and (g)–(h) DAY+1. No CLAUS data is available before 1983, so that these composites consist of only 35 events. Black boxes mark the study area. Note the different geographical areas in the right and left panels.

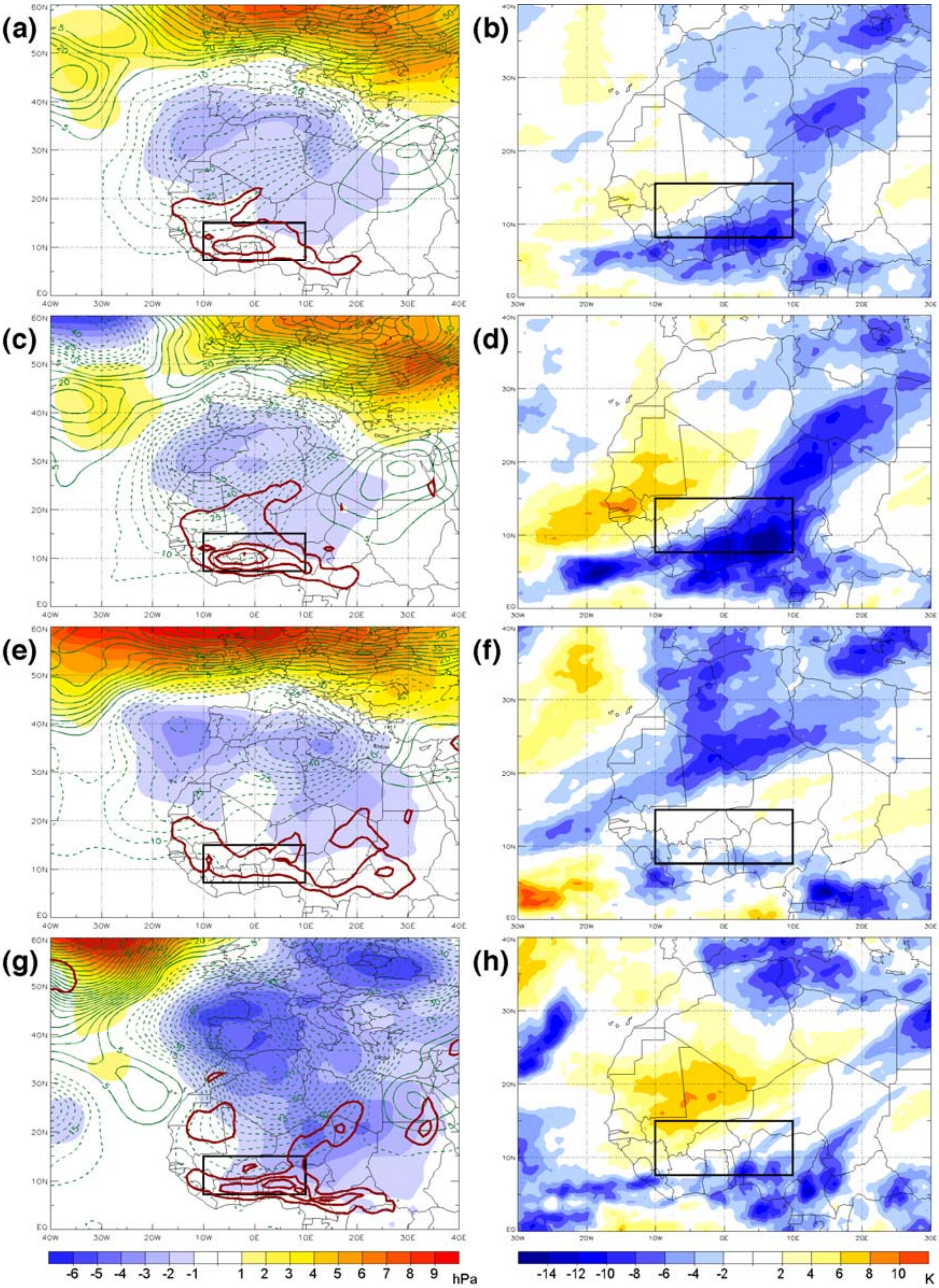
(a)
(b)
(c)
(d)
(e)
(f)
(g)
(h)
-6 -5 -4 -3 -2 -1 1 2 3 4 5 6 7 8 9 hPa
-14 -12 -10 -8 -6 -4 -2 2 4 6 8 10 K

FIG. 12. Composited anomalies of analyzed Z500 (contoured every 5 gpm), MSLP (shaded), and TD2M (red contours showing 2, 4, 6, and 8 °C) (left panels), as well as CLAUS BTs (right panels) for DAY0 over (a)–(b) all 43 wet events, (c)–(d) all 23 hits, (e)–(f) all 20 misses, and (g)–(h) all 11 false alarms. No CLAUS data is available before 1983, so that these composites consist of 35 events in (b), 20 events in (d), and 15 events in (f). The false alarms are not affected. Black boxes mark the study area. Note the different geographical areas in the right and left panels.

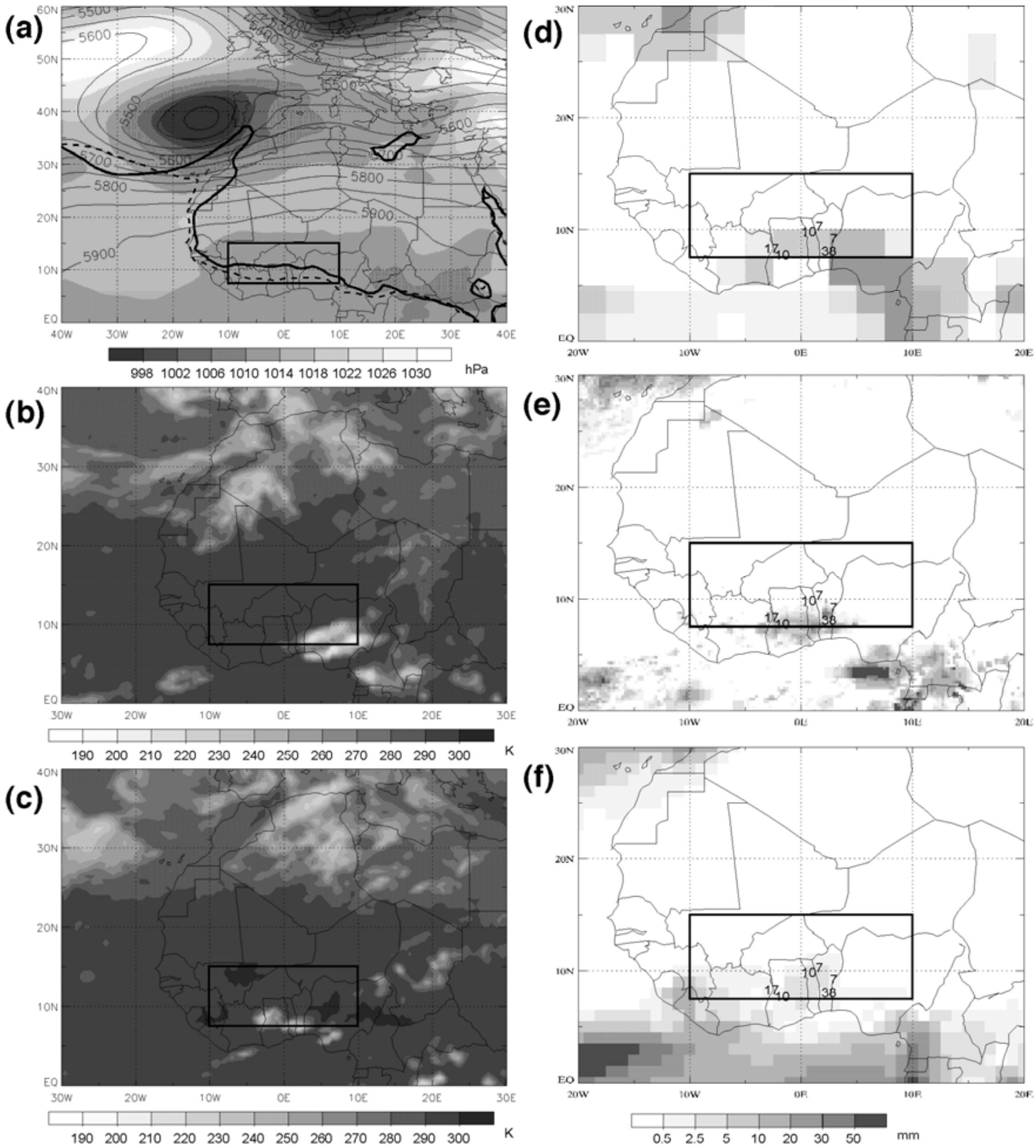

FIG. 13. Example of a forecast miss. (a) Analyzed Z500 (contours every 50 gpm), MSLP (shading), and 14°C contour of TD2M (thick solid line) at 1200 UTC 02 Feb. 1998. The dashed line shows the 1979–2002 February average of the latter contour as a reference. (b)–(c) CLAUS IR brightness temperatures at 2100 UTC on 01 and 02 February, respectively. (d)–(f) as Fig. 1 but for 31 Jan. – 04 Feb. 1998. Black boxes mark the study area.

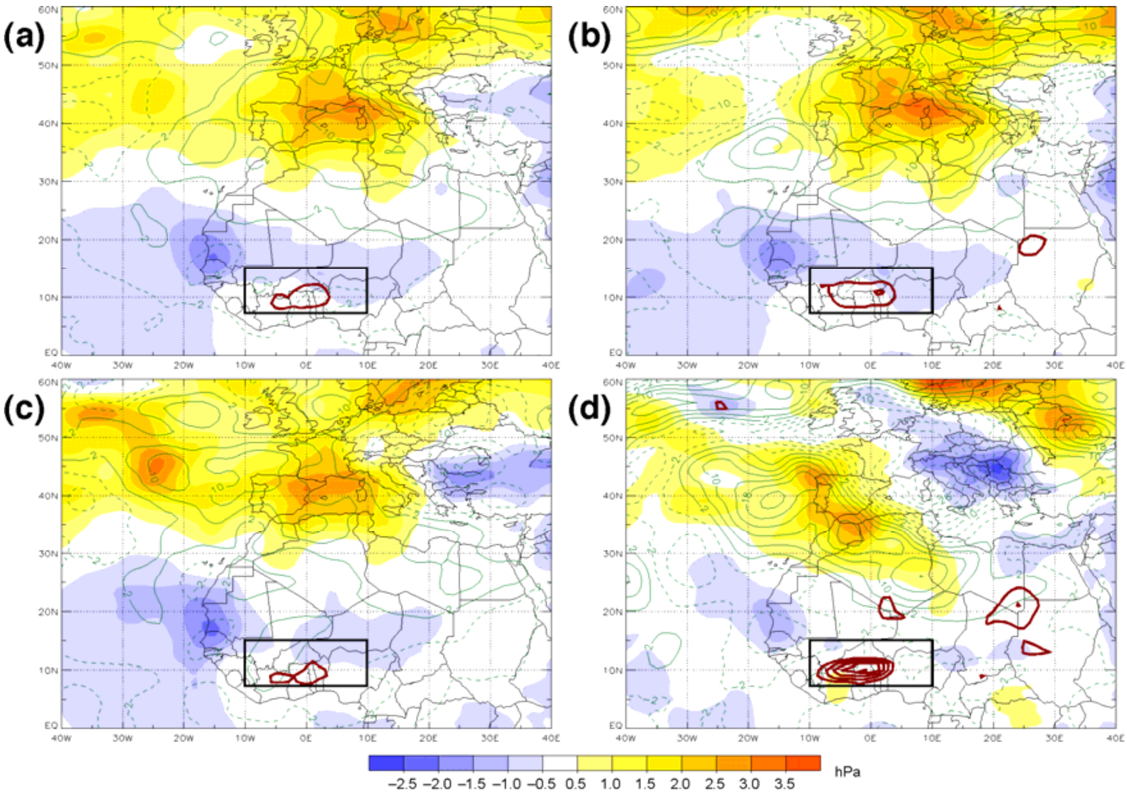

FIG. 14. Composited differences of Z500 (green contours every 4 gpm), MSLP (shaded), and TD2M (red contours showing 2, 4, 6, 8, and 10°C) between ERA-40 60-hour forecasts and the corresponding re-analysis for DAY 0: (a) all 43 wet events, (b) all 23 hits, (c) all 20 misses, and (d) all 11 false alarms. Black boxes mark the study area.

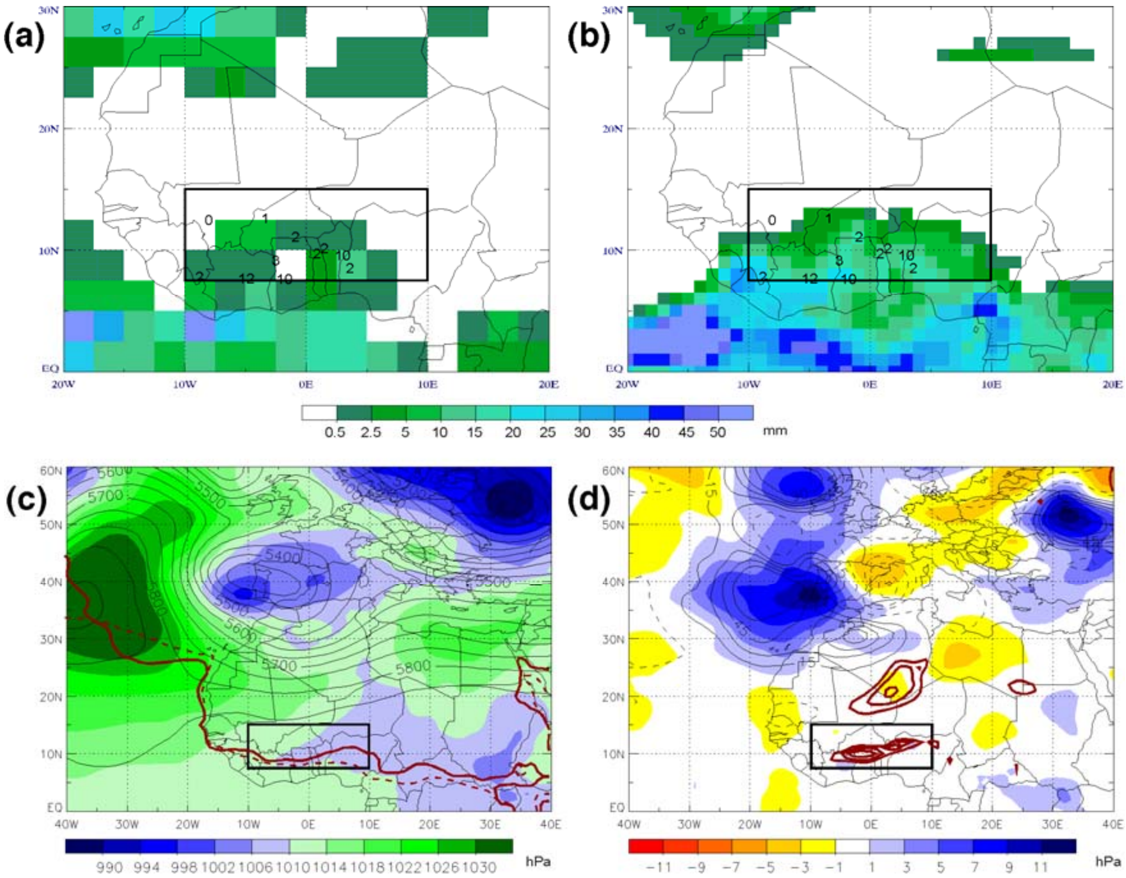

FIG. 15. Example of a false alarm. (a)–(b) As Figs. 1a and 1c but for 15–19 Feb. 1991. (c) Z500 (contours every 50 gpm), MSLP (shading), and 14°C contour of TD2M (red solid line) at 1200 UTC 17 Feb. 1991. The dashed red line shows the 1979–2002 February average of the latter contour as a reference. (d) Differences of Z500 (contoured every 15 gpm), MSLP (shaded), and TD2M (red contours showing 6, 10, and 14°C) between the ERA-40 60-hour forecast valid at 1200 UTC 17 Feb. 1991 and the corresponding re-analysis. Black boxes mark the study area.